

Numerical Investigation Effectiveness of Adiabatic Film Cooling of Gas Turbine Blades

Vishnu T Pillai, Jayakumar J S

Dept. of Mechanical Engineering

Amrita Vishwa Vidyapeetham, Amritapuri Kollam, India

vishnu.vtp@gmail.com

jsjayan@am.amrita.edu

Giridhara Babu Y

Propulsion Division

CSIR-National Aerospace Laboratory Bangalore, India

giris@nal.res.in

Abstract — This study aims at numerically investigating the film cooling effectiveness of gas turbine blades. The study is done on the leading edge of a gas turbine blade having five rows of holes. The holes are such that one is at the stagnation line, two are at 30 deg and other two are at 60 deg on either side of the stagnation line. Each row as five holes with a hole diameter of 3mm, 4mm and 5.6mm at a pitch of 21mm and the holes are oriented at an angle of 30 degrees with respect to the stream line direction. The rows of film cooling holes are arranged in a staggered manner to cover more flow area on the blade surface. Numerical investigation is done by varying the blowing ratios (B.R). The BR used in this analysis are 0.75, 1.25 and 1.75. The BR is varied by varying the coolant mass flow while maintaining the main flow constant. The film cooling effectiveness is also estimated using the CFD simulation. The blade leading edge is designed using Solid Works and the meshing is done using ANSYS-Workbench. ANSYS-FLUENT is used as the solver. The k-epsilon realizable turbulence model is used to solve the flow field.

Keywords — Gas Turbine, film cooling, Blowing Ratio, CFD, Heat transfer

I. INTRODUCTION

In day to day life gas turbines are used in different applications such as aircraft propulsion, electric power generation etc. As a result, the demand to improve the performance of the gas turbine blade, we have to increase the inlet temperature of the gas entering the turbine. So when the performance of the gas turbine is increased by this method, we face a problem that the inlet temperatures are much higher than the melting temperature of the available alloys used to make the turbine blades. However, to overcome this problem we need to cool the turbine blade simultaneously. Film cooling is one of the effective techniques used for this

purpose. Fig.1 shows the film cooling concept. Film cooling involves injection of jet of cooled air through rows of holes in the surface of the blade, providing a thin layer of cool air on the downstream of the film cooling hole. This insulates the blade from hot mainstream flow and acts as a heat sink to cool the blade surfaces.

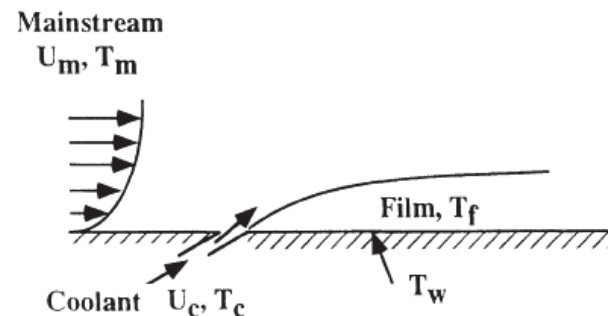


Fig. 1 Film Cooling Concept.

Hams and Lylek [1] studied the effect of various film hole geometries on flow and thermal characteristics, and the dominant mechanisms responsible for differences in these characteristics are observed. Fig.2 shows the five distinct film cooling configurations. They are: (1) cylindrical film hole, (2) forward-diffused film hole, (3) laterally diffused film hole, (4) inlet shaped film hole, and (5) cusp-shaped film hole on a flat plate.

The film holes in this study are at an injection angle 35 deg, $L/D=4$ and Blowing ratio (BR) = 1.25 & 1.88. Blowing ratio is one of the most important parameter in film cooling and it is defined as the ratio of coolant mass flux ratio to the mainstream mass flux ratio.

$$\text{Blowing Ratio, BR} = \frac{\rho_c U_c}{\rho_m U_m} \quad (1)$$

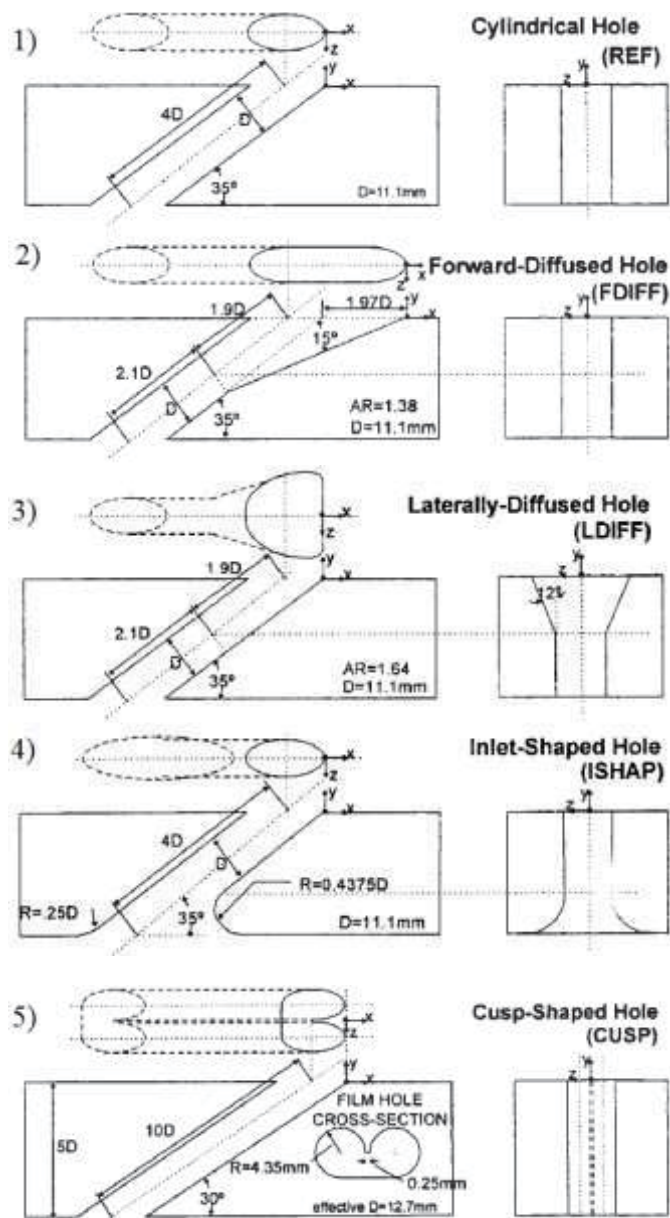


Fig. 2 Schematic of selected film holes shows the geometry of each configuration (Hyams and Leylek [1])

As per the geometry taken into consideration, cylindrical hole & laterally diffused hole do not have significant impact on the film cooling performance. Out of the configurations tested, it is observed that the laterally diffused hole configuration is having the best film cooling performance.

Shaohua et al. [2] documented numerical simulation of turbine blade film cooling with different blowing ratios and pitch as using *k*-epsilon turbulence model. They observed that, the model gave the temperature field of different hole in rows located on the leading edges of turbine blade. They compared the film cooling effectiveness on various blowing ratios and hole to hole spacing. They concluded that the cooling efficiency is directly proportional to the blowing ratio up to a certain value. Further increase in the blowing ratio results in a

decrease in the film cooling efficiency. They also found that, the effective cooling area covered by cooling holes of smaller pitch is better than the cooling area covered by larger pitch.

Ken-ichi Funazaki et al. [3] studied the effect of free stream turbulence on leading edge film cooling. They calculated the heat transfer coefficient and the adiabatic film effectiveness of turbine blade. The film cooling effectiveness is calculated using the relation,

$$\eta = \frac{T_m - T_w}{T_m - T_c} \quad (2)$$

where, T_m , T_w and T_c , represent main stream temperature, adiabatic wall temperature and coolant temperature respectively. The study was done with several test case of different blowing ratios and three main stream turbulence intensities.

Geometry of the test model used in this study consists of a semicircular part of 80 mm diameter and a flat plate of 100 mm in length and 280 mm in height. The injection angles taken were 0, 25, 55 degree in the spanwise direction. In this study thermocouple rake was used to perform temperature measurement within planes normal to surface face. The thermocouple rake consists of 13 K-type thermocouples. They used two types of leading edge models with cylindrical and diffuser holes. The results showed that the effect of mainstream turbulence intensity was significantly high in case of diffuser hole. It was also observed that the average film effectiveness decreased in the span wise direction of the blade. For numerical simulation, commercial software ANSYS CFX 12 was used in this study. Time averaged Reynolds-Averaged Navier-Stokes (RANS) approach using Shear-Stress Transport (SST) two-equation model was employed to solve the flow field.

TarekElnady et al. [4] studied two types of hole geometries viz., one with 2d expanded hole at exit at an angle of 90° and the other with 4d expanded hole at exit at an angle of 60°. The angle was measured with respect to blade surface on the leading edge and the pitch to diameter ratio (P/d) was 4.5 for both the geometries. They found that, for the same blowing ratio, the 4d expanded-60° inclined hole configuration had higher cooling effectiveness than all other geometries tested. They used 4 blowing ratios: 1, 1.35, 1.7, and 2. The Mach number and Reynolds number used for their study were 0.23 & 1.4e5 respectively. The cascade inlet velocity which corresponds to Mach number 0.23 is 85 m/s. They concluded that, the smooth expansion hole shows higher effectiveness when compared with standard cylindrical hole.

Kim and Kim [5] studied the influence of shaped injection holes on flow characteristic of film cooling on the leading edge of turbine blades. Five different cylindrical models with various injection holes, were used for the study. The type of hole are the base line cylindrical hole, laid back (spanwise-diffused) holes and tear drop shaped (spanwise-and stream wise-diffused) hole respectively. Results show that the conventionally cylindrical holes have poor film cooling performance as compared to the shaped holes.

It was seen that the laidback hole provides better film cooling performance than the other holes. The film cooling performance can be significantly improved by controlling the

injection hole shape. The laidback holes show much higher film cooling effectiveness. The model used in this is made of polyacetal, which has low thermal conductivity of 0.15 W/m K. The model consist of three staggered rows (nine holes in each row) with a leading edge diameter of $D=80$ mm and injection angle of 30 degree relative to the spanwise direction. The others holes are same in shape except the exit is opened by 10 deg in the spanwise direction.

From the above mentioned literature surveys, it is found that the optimization of turbine blade leading edge film cooling requires the investigation of various flow and geometrical conditions like hole inclination angle, hole shape, hole location, diameter of the hole, hole angle with respect to leading edge surface, coolant to mainstream blowing ratio and density ratio (D.R). Among these parameters hole shape, hole inclination angle and blowing ratio have significant effect on the film cooling effectiveness. Thus study aims at investigating the film cooling effectiveness numerically for the scaled up gas turbine leading edge blade model.

II. COMPUTATIONAL METHODOLOGY AND PROCEDURE

Film cooling effectiveness for different blowing ratios of 0.75, 1.25 and 1.75 were numerically studied using ANSYS Fluent. For this study, cylindrical hole with 30 deg hole orientation angle was considered. The computational model has three rows of five holes at 30 deg. angle from the stagnation line with 21mm pitch in staggered manner. The model is designed in such a manner that it consist of three different models with different film cooling hole diameter of 3mm, 4mm and 5.6mm. The turbulence model used in this analysis was *k*-epsilon Realizable model with enhanced wall function.

A. Model Description

The leading edge part of the turbine blade is designed using SolidWorks. Model description of the leading edge part of the blade is listed in Table 1. Three different models are developed for the study.

Table 1 Turbine Blade Leading Edge Model Description.

Sl. No	Model description	Dimensions
1	Leading Edge Outer Diameter	89 mm
2	Leading Edge Inner Diameter	65 mm
3	Film Cooling Hole Diameter	3mm, 4mm and 5.6mm
4	Leading Edge Model Height	210 mm
5	No. Holes / Row	5
6	Hole Orientation Angle	30 Deg angle from the Stagnation line

Fig.3 shows the geometrical representation of the leading edge of turbine blade model with different hole diameters.

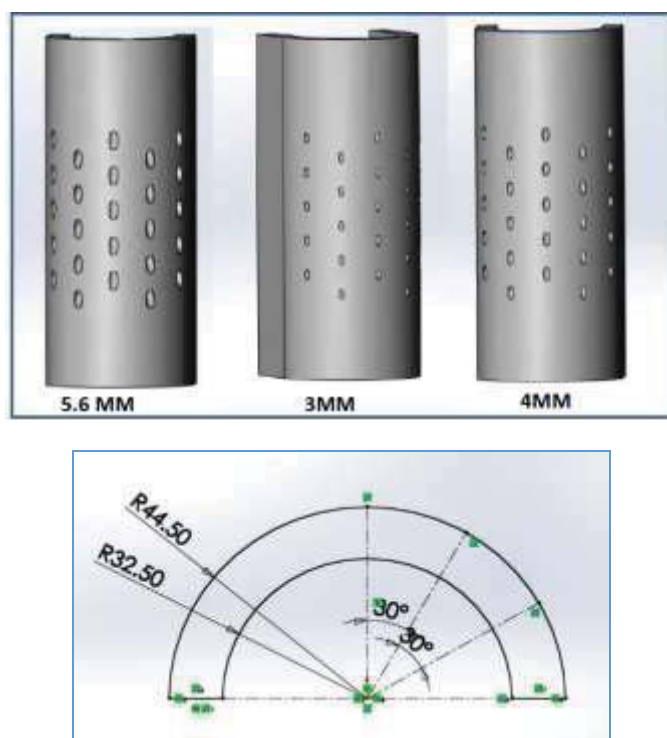


Fig. 3 Geometry of the Computational Model

B. Geometry of the Computational Model

The computational model consists of leading edge of gas turbine blade with the flow duct having a size of 300 x 210 x 210 mm. Outer and inner diameter of leading edge is 89mm and 65mm respectively as shown in Fig. 4. Fig.5 shows the leading edge of the turbine blade having five rows of holes. The holes are such that one is at the stagnation line, two are at 30 deg and other two are at 60 deg on either side of the stagnation line. Each row has the five holes at a pitch of 21mm with the hole angles of 30 degrees oriented with the stream line direction. The film cooling holes are arranged in a staggered manner to cover more area on the blade surface. The diameter of holes considered in this analysis are 3mm, 4mm and 5.6mm. Computational domain is made according to the experimental test section, such that only half of length of the test section is considered to reduce number of element cells and reduce simulation time. Computational model is prepared using solidWorks and ANSYS Workbench.

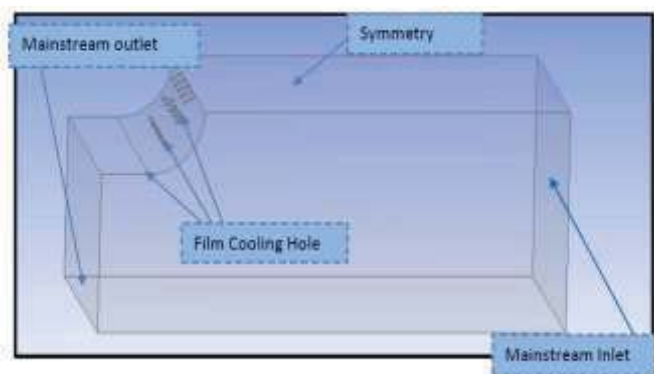


Fig. 4 Computational domain

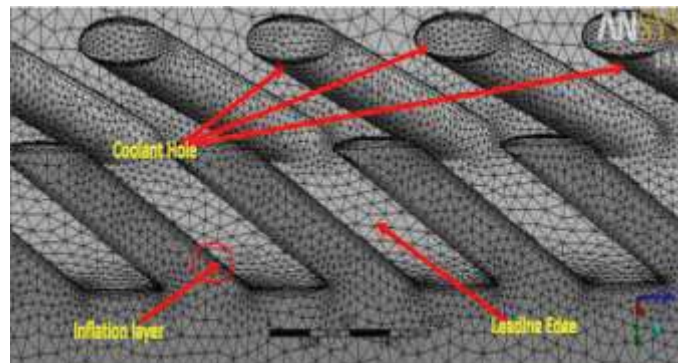


Fig. 7 Grid generation of film cooling holes with gas turbine leading edge

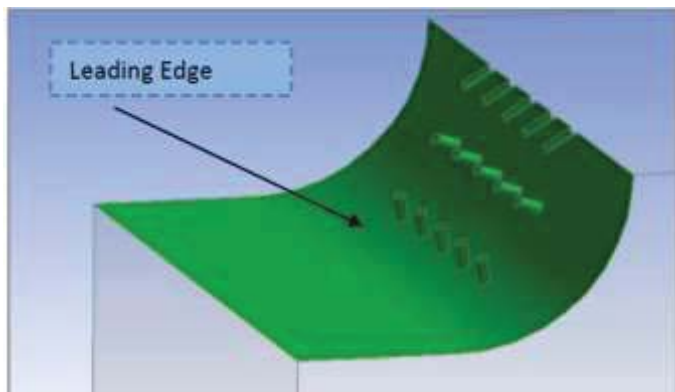


Fig. 5 Film cooling hole with gas turbine leading edge

C. Grid Generation

Meshing of the computational domain is done using ANSYS Workbench. The blade leading edge structure along with the flow area is discretized using tetrahedral volume mesh. Fig.6 shows generated grid for the computational model. Tetrahedron meshes are constructed for the whole domain with smooth inflation with maximum 5 layers on the boundary of leading edge. Fine meshing is used here.

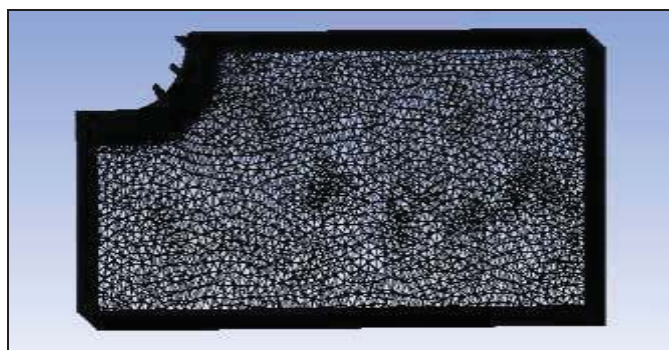


Fig. 6 Grid generation of computational model

The enlarged view of grid at the leading edge part is shown in Fig.7. The figure also shows the inflation layer in the coolant hole.

Grid independency test was done in the order to determine the correct mesh volumes that are needed to be provided for the geometry. It depends on the sizing function assigned for the domain as a whole and also for individual components. Specific size function is assigned for a particular region such as leading edge. The sizing function depends on the complexity and the type of meshing required for the geometry. For the present case, since the meshing for all the geometries are the same, grid independency is conducted for only one model. The end result of the test will determine a size function which brings about least computational effort, at the same time accurate results. If the design parameter does not change even after increasing the number of cell above a particular limit, the cell size with least volume can be selected for the meshing.

Analysis was conducted with four mesh volumes, viz., 547637, 705526, 1212837 and 2023379, of the computational domain. For the considered number of elements, the mesh with 705526 cells and higher showed same film cooling effectiveness as shown in Fig 8. Hence the lowest mesh size i.e., 705526 cells is considered suitable for all the further studies.

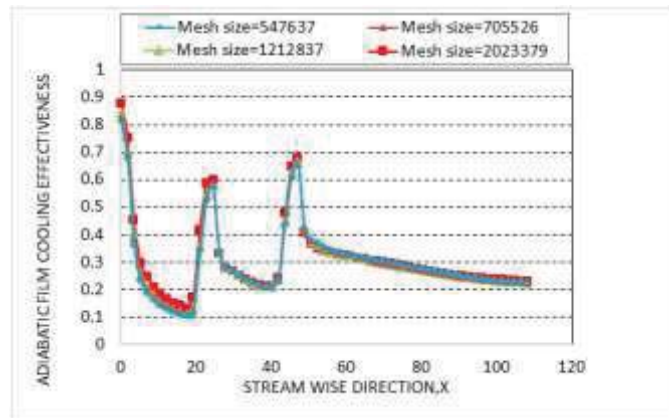


Fig. 8 Grid independency test

This mesh size will provide accurate results while reducing the time for computation. Hence the best mesh volume for the present geometry was selected on the basis of grid independency test.

D. Boundary Condition

The types of boundary conditions applied for the computational study are shown in the Table 2.

Table 2: Boundary Condition

	NAME	BOUNDARY TYPE
1	Main Stream Inlet	Pressure Inlet
2	Mainstream outlet	Pressure Outlet
3	Coolant Inlet	Pressure Inlet
4	Wall	Wall
5	Leading Edge	Wall

The ANSYS FLUENT was set to run with double precision. A pressure based solver is used in the fluent system. The $k-\epsilon$ realizable turbulence model is used for the CFD simulation.

III. GOVERNING EQUATION

The governing equations relating to the problem are implemented in ANSYS framework. The governing equations are the conservation, momentum and energy equations.

A. Continuity equation:

From the law of conservation of mass law comes the continuity equation

$$\frac{\partial \rho}{\partial t} + \frac{\partial(\rho V_x)}{\partial x} + \frac{\partial(\rho V_y)}{\partial y} + \frac{\partial(\rho V_z)}{\partial z} = 0 \tag{3}$$

V_x, V_y and V_z , denotes the components of the velocity vector in the x, y and z direction

B. Momentum Equation

X direction

$$\frac{\partial(\rho V_x)}{\partial t} + \frac{\partial(\rho V_x V_x)}{\partial x} + \frac{\partial(\rho V_y V_x)}{\partial y} + \frac{\partial(\rho V_z V_x)}{\partial z} = \tag{4}$$

$$\rho g_x - \frac{\partial P}{\partial x} + R_x + \frac{\partial}{\partial x} \left(\mu_e \frac{\partial V_x}{\partial x} \right) + \frac{\partial}{\partial y} \left(\mu_e \frac{\partial V_x}{\partial y} \right) + \frac{\partial}{\partial z} \left(\mu_e \frac{\partial V_x}{\partial z} \right) + T_x$$

Y direction

$$\frac{\partial(\rho V_y)}{\partial t} + \frac{\partial(\rho V_x V_y)}{\partial x} + \frac{\partial(\rho V_y V_y)}{\partial y} + \frac{\partial(\rho V_z V_y)}{\partial z} = \tag{5}$$

$$\rho g_y - \frac{\partial P}{\partial y} + R_y + \frac{\partial}{\partial x} \left(\mu_e \frac{\partial V_y}{\partial x} \right) + \frac{\partial}{\partial y} \left(\mu_e \frac{\partial V_y}{\partial y} \right) + \frac{\partial}{\partial z} \left(\mu_e \frac{\partial V_y}{\partial z} \right) + T_y$$

Z direction

$$\frac{\partial(\rho V_z)}{\partial t} + \frac{\partial(\rho V_x V_z)}{\partial x} + \frac{\partial(\rho V_y V_z)}{\partial y} + \frac{\partial(\rho V_z V_z)}{\partial z} = \tag{6}$$

$$\rho g_z - \frac{\partial P}{\partial z} + R_z + \frac{\partial}{\partial x} \left(\mu_e \frac{\partial V_z}{\partial x} \right) + \frac{\partial}{\partial y} \left(\mu_e \frac{\partial V_z}{\partial y} \right) + \frac{\partial}{\partial z} \left(\mu_e \frac{\partial V_z}{\partial z} \right) + T_z$$

g_x, g_y and g_z , components of acceleration due to gravity

μ_e , effective viscosity

R_x, R_y and R_z represents source term.

T_x, T_y and T_z represents viscous loss term

$$T_x = \frac{\partial}{\partial x} \left(\mu \frac{\partial V_x}{\partial x} \right) + \frac{\partial}{\partial y} \left(\mu \frac{\partial V_y}{\partial x} \right) + \frac{\partial}{\partial z} \left(\mu \frac{\partial V_z}{\partial x} \right) \tag{7}$$

$$T_y = \frac{\partial}{\partial x} \left(\mu \frac{\partial V_x}{\partial y} \right) + \frac{\partial}{\partial y} \left(\mu \frac{\partial V_y}{\partial y} \right) + \frac{\partial}{\partial z} \left(\mu \frac{\partial V_z}{\partial y} \right) \tag{8}$$

$$T_z = \frac{\partial}{\partial x} \left(\mu \frac{\partial V_x}{\partial z} \right) + \frac{\partial}{\partial y} \left(\mu \frac{\partial V_y}{\partial z} \right) + \frac{\partial}{\partial z} \left(\mu \frac{\partial V_z}{\partial z} \right) \tag{9}$$

C. Energy Equation

$$\frac{\partial}{\partial t} (\rho c_p T_0) + \frac{\partial}{\partial x} (\rho V_x c_p T_0) + \frac{\partial}{\partial y} (\rho V_y c_p T_0) + \frac{\partial}{\partial z} (\rho V_z c_p T_0) \tag{10}$$

$$= \frac{\partial}{\partial x} \left(k \frac{\partial T_0}{\partial x} \right) + \frac{\partial}{\partial y} \left(k \frac{\partial T_0}{\partial y} \right) + \frac{\partial}{\partial z} \left(k \frac{\partial T_0}{\partial z} \right) + W^v + E^k + \phi + \frac{\partial p}{\partial t}$$

The viscous work term is

$$W^v = V_x \mu \left[\frac{\partial^2 V_x}{\partial x^2} + \frac{\partial^2 V_x}{\partial y^2} + \frac{\partial^2 V_x}{\partial z^2} + \frac{\partial}{\partial x} \left(\frac{\partial V_x}{\partial x} + \frac{\partial V_y}{\partial y} + \frac{\partial V_z}{\partial z} \right) \right] + \tag{11}$$

$$V_y \mu \left[\frac{\partial^2 V_y}{\partial x^2} + \frac{\partial^2 V_y}{\partial y^2} + \frac{\partial^2 V_y}{\partial z^2} + \frac{\partial}{\partial x} \left(\frac{\partial V_x}{\partial x} + \frac{\partial V_y}{\partial y} + \frac{\partial V_z}{\partial z} \right) \right] +$$

$$V_z \mu \left[\frac{\partial^2 V_z}{\partial x^2} + \frac{\partial^2 V_z}{\partial y^2} + \frac{\partial^2 V_z}{\partial z^2} + \frac{\partial}{\partial x} \left(\frac{\partial V_x}{\partial x} + \frac{\partial V_y}{\partial y} + \frac{\partial V_z}{\partial z} \right) \right]$$

The kinetic energy term is

$$E^k = - \frac{\partial}{\partial x} \left[\frac{k}{c_p} \frac{\partial}{\partial x} \left(\frac{1}{2} |V^2| \right) \right] - \frac{\partial}{\partial y} \left[\frac{k}{c_p} \frac{\partial}{\partial y} \left(\frac{1}{2} |V^2| \right) \right] \tag{12}$$

$$- \frac{\partial}{\partial z} \left[\frac{k}{c_p} \frac{\partial}{\partial z} \left(\frac{1}{2} |V^2| \right) \right]$$

The viscous dissipation term is

$$\phi = 2\mu \left[\left(\frac{\partial V_x}{\partial x} \right)^2 + \left(\frac{\partial V_y}{\partial y} \right)^2 + \left(\frac{\partial V_z}{\partial z} \right)^2 \right] + \tag{13}$$

$$\mu \left[\left(\frac{\partial V_y}{\partial x} + \frac{\partial V_x}{\partial y} \right)^2 + \left(\frac{\partial V_z}{\partial y} + \frac{\partial V_y}{\partial z} \right)^2 + \left(\frac{\partial V_x}{\partial z} + \frac{\partial V_z}{\partial x} \right)^2 \right]$$

D. Turbulence Model

The standard $k-\epsilon$ model is based on model transport equations for the turbulence kinetic energy (k) and its dissipation rate (ϵ). The turbulent kinetic energy equation is

$$\frac{\partial \rho k}{\partial t} + \frac{\partial(\rho V_x k)}{\partial x} + \frac{\partial(\rho V_y k)}{\partial y} + \frac{\partial(\rho V_z k)}{\partial z} \tag{14}$$

$$= \frac{\partial}{\partial x} \left(\frac{\mu_t}{\sigma_k} \frac{\partial k}{\partial x} \right) + \frac{\partial}{\partial y} \left(\frac{\mu_t}{\sigma_k} \frac{\partial k}{\partial y} \right) + \frac{\partial}{\partial z} \left(\frac{\mu_t}{\sigma_k} \frac{\partial k}{\partial z} \right) +$$

$$\mu_t \phi - \rho \epsilon + \frac{C_4 \beta \mu_t}{\sigma_t} \left(g_x \frac{\partial T}{\partial x} + g_y \frac{\partial T}{\partial y} + g_z \frac{\partial T}{\partial z} \right)$$

The Dissipation Rate

$$\frac{\partial \rho \epsilon}{\partial t} + \frac{\partial (\rho V_x \epsilon)}{\partial x} + \frac{\partial (\rho V_y \epsilon)}{\partial y} + \frac{\partial (\rho V_z \epsilon)}{\partial z}$$

$$= \frac{\partial}{\partial x} \left(\frac{\mu_t}{\sigma_\epsilon} \frac{\partial \epsilon}{\partial x} \right) + \frac{\partial}{\partial y} \left(\frac{\mu_t}{\sigma_\epsilon} \frac{\partial \epsilon}{\partial y} \right) + \frac{\partial}{\partial z} \left(\frac{\mu_t}{\sigma_\epsilon} \frac{\partial \epsilon}{\partial z} \right) + C_{1\epsilon} \mu_t \frac{\epsilon}{k} \phi - C_{2\epsilon} \rho \frac{\epsilon^2}{k} + \frac{C_\mu (1 - C_3) \beta \rho k}{\sigma_t} \left(g_x \frac{\partial T}{\partial x} + g_y \frac{\partial T}{\partial y} + g_z \frac{\partial T}{\partial z} \right) \quad (15)$$

A second-order upwind scheme was used for the calculations. The convergence criteria for dependent variables like continuity, momentum, energy etc. are specified as 10^{-5} . The under-relaxation factors shown in Table 3 are used in this work.

Table 3 Under relaxation factor

Factors	Values
Pressure	0.3
Density	1
Body Force	1
Momentum	0.6
Turbulent Kinetic Energy	0.8
Turbulent Dissipation rate	0.8
Energy	1

The simulation is done with the COUPLED algorithm. It solves the momentum and pressure-based continuity equations together. The full implicit coupling is achieved through an implicit discretization of pressure gradient terms in the momentum equations and an implicit discretization of the face mass flux.

The simulation is done in parallel mode of a system having quad core Intel® Core™ i5 processor. The calculations are done over a 1500 iterations to get the converged results in a 16GB RAM system. Converged result was obtained within time duration of three hours.

IV. RESULT AND DISCUSSION

The Film temperature on the leading edge surface numerically obtained by varying the blowing ratios as 0.75, 1.25 and 1.75. Adiabatic film cooling effectiveness is numerically obtained for gas turbine blades with hole diameter of 3mm, 4mm and 5.6mm where the injection angle is oriented at 30 deg with respect to the blade surface. The adiabatic film effectiveness versus streamwise direction at BR= 0.75, 1.25, and 1.75 for 5.6mm model is shown in Fig. 9. Streamwise direction is the direction along the mainstream flow.

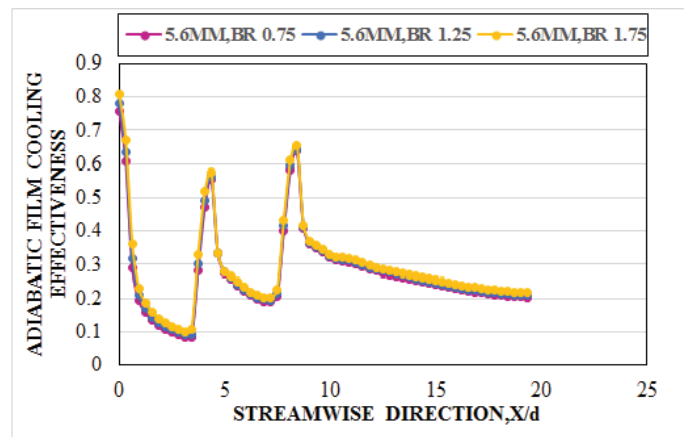


Fig. 9 Numerically Evaluated Adiabatic Film Cooling Effectiveness at the Blowing Ratio of 0.75, 1.25 and 1.75 for 5.6mm hole model at 30deg. angle models.

High adiabatic film cooling effectiveness is seen for blowing ratio of 1.75 than blowing ratios of 1.25 and 0.75. Film temperature contours for 5.6mm models are obtained by varying the blowing ratios. By using this results, surface film temperature values was estimated which was subsequently used to calculate the cooling. The temperature contours of 5.6mm for different blowing ratios are shown in Fig 10 to 12.

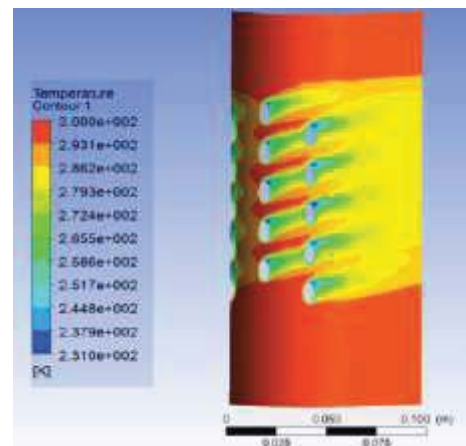


Fig. 10 Temperature Contours, for 5.6mm coolant hole diameter model at B.R.=0.75.

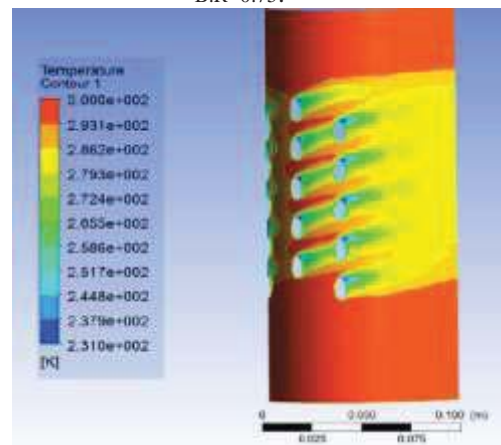


Fig. 11 Temperature Contours, for 5.6mm coolant hole diameter model at B.R=1.25.

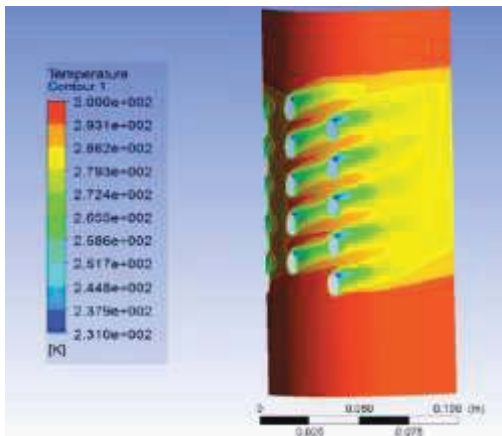


Fig. 12 Temperature Contours, for 5.6mm coolant hole diameter model at B.R=1.75.

From the temperature contours it is seen that the film cooling reduces temperature near the holes. From Fig. 12 it can be seen that the film cooling effectiveness high for B.R = 1.75.

The adiabatic film effectiveness at BR 0.75, 1.25 and 1.75 for 4mm model is shown in Fig. 13.

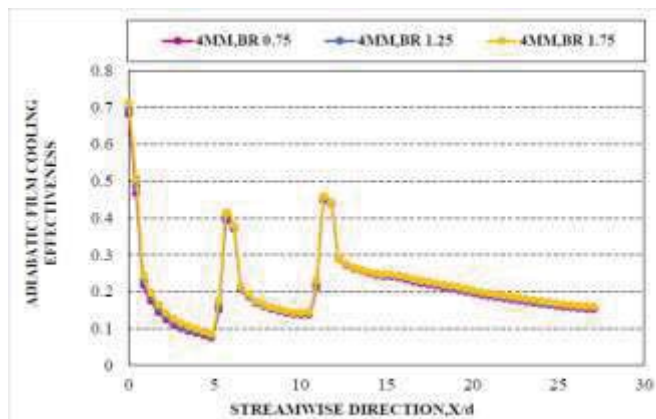


Fig. 13 Numerically Evaluated Adiabatic Film Cooling Effectiveness at the Blowing Ratio of 0.75, 1.25 and 1.75 for 4mm hole model at 30deg. angle.

The adiabatic film effectiveness at BR 0.75, 1.25, and 1.75 for 3mm model is shown in Fig. 14.

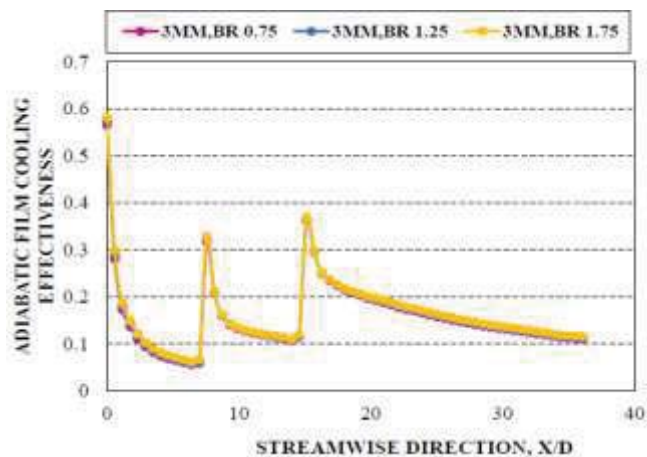


Fig. 14 Numerically Evaluated Adiabatic Film Cooling Effectiveness at the Blowing Ratio of 0.75, 1.25 and 1.75 for 3mm hole model at 30deg. angle

It is observed that film cooling effectiveness has increased with increase in blowing ratio. On further increasing blowing ratio, not much increase in cooling effectiveness was obtained.

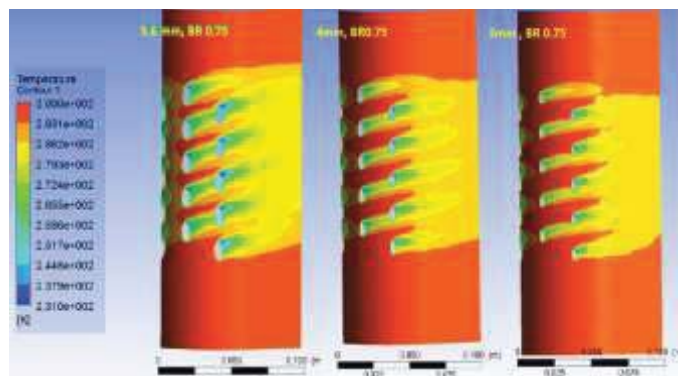


Fig. 15 Temperature Contours, for 5.6mm, 4mm and 3mm Coolant hole diameter model at B.R=0.75

Fig 15 shows temperature contours of 5.6mm, 4mm and 3mm model at B.R of 0.75. This figure shows that by varying hole diameter from 3mm to 5.6mm, the 5.6 mm hole diameter blade shows better coolant flow spread throughout the surface of the blade.

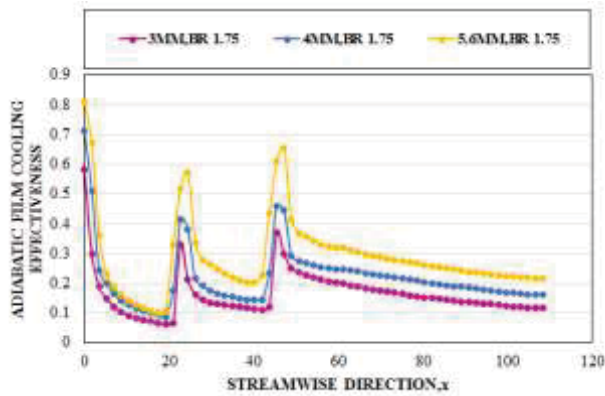


Fig. 16 5.6mm, 4mm and 3mm coolant hole diameter with blowing ratio of 1.75

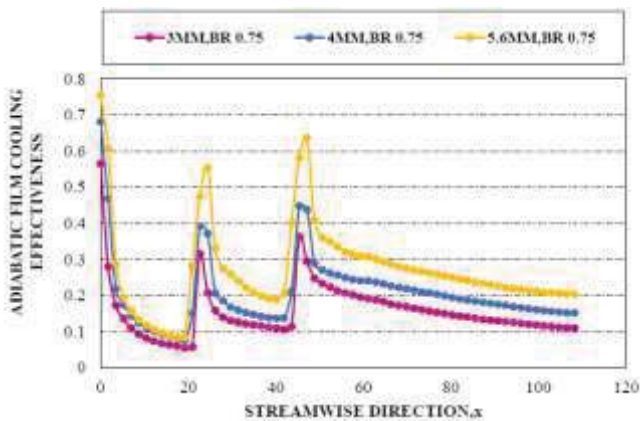


Fig. 17 5.6mm, 4mm and 3mm coolant hole diameter with blowing ratio of 0.75

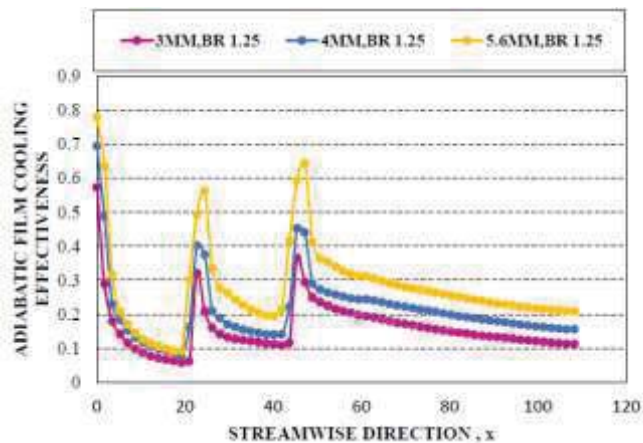


Fig. 18 5.6mm, 4mm and 3mm coolant hole diameter with blowing ratio of 1.25

Fig 16 to 18 show comparison of cooling effectiveness as a function of hole diameter for the same blowing ratio. From these graphs it is observed that 5.6mm hole diameter gives high adiabatic film cooling effectiveness for all blowing ratios.

V. CONCLUSION

This study aims at investigating the film cooling effectiveness of the leading edge of a gas turbine blade with

five rows of film cooling holes. From CFD estimation, the cooling effectiveness is found to be increasing with the increase in blowing ratio from 0.75 to 1.75. On further increase in blowing ratios it did not show any considerable improvement. It is also found that the blowing ratio 1.75 is optimized. The hole diameter from 3mm to 5.6mm we observed that 5.6mm hole diameter gives the maximum adiabatic film cooling effectiveness.

Acknowledgment

The authors wish to thank Director, NAL, Bangalore for permitting this work to be done at NAL. The authors are grateful to Dr. M Jayaraman, Head, and Propulsion Division for allowing to undertake the work at propulsion Division, CSIR-NAL and Mr. J Felix, Scientist, CSIR-NAL for his support.

Nomenclature

A	Area, m ²
B.R	Blowing Ratio
c_p	Specific heat, J/kgK
D.R	Density Ratio
D	Diameter of the leading edge model, mm
d	Diameter of Film cooling Hole, mm
deg.	Degrees
g_x, g_y and g_z	Components of acceleration due to gravity, m/s ²
\bar{g}_x, \bar{g}_y and \bar{g}_z	Components of acceleration due to gravity, m/s ²
h	Heat transfer coefficient, W/m ² K
k_e	Effective conductivity, W/mK
k	Thermal conductivity, W/mK
M	Mass Flow, kg/s
P	Pressure, Pa
T	Temperature, K
v	Velocity, m/s
R_x, R_y and R_z	Distributed resistance
T_x, T_y and T_z	viscous loss term
V_x, V_y and V_z	Components of the velocity vector in the x, y and z direction
T_0	Total (or stagnation) temperature, K
W^v	Viscous work term, J
Q^v	Volumetric heat source, W/m ³
E^k	Kinetic Energy, J
Greek Symbols	
η	Adiabatic film Cooling Effectiveness
ρ	Density, kg/m ³
μ_e	Effective viscosity, kg/ms
Φ	Viscous heat generation term, J

Subscripts

c Coolant
f Film
m Mainstream
w Wall
x,y,z Global Cartesian coordinates

References

- [1] D.G Hyams and J H Leylek, "A Detailed Analysis of film cooling physics: streamwise injection with shaped holes", Journal of turbomachinery, 2000 volume 122/133
- [2] LI Shaohua Tao Peng, Li- Xian Liu, Ting-ting GUO , Bin Yuan "Numerical Simulation of Turbine Blade Film cooling with Different Blowing Ratio and Hole to hole space" International Conference on Power Engineering, Oct 23-27, 2007
- [3] Ken-ichi Funazaki, Hirokazu Kawabata and Yoji Okita "Free-Stream Turbulence Effects on Leading Edge Film Cooling" International Journal of Gas Turbine, Propulsion and Power System. February 2012, Volume 4, Number 1
- [4] Tarek Elnady, Ibrahim Hassan, Lyse Kadem and Terry Lucas "Cooling effectiveness of shaped film holes for leading edge" Experimental Thermal and Fluid Science 44 (2013) 649–661
- [5] Youn J. Kim , S.M. Kim, "Influence of shaped injection holes on turbine blade leading edge film cooling", International Journal of Heat and Mass Transfer 47 (2004) 245–256